PAPER

ZnO dense nanowire array on a film structure in a single crystal domain texture for optical and photoelectrochemical applications

To cite this article: Miao Zhong *et al* 2012 *Nanotechnology* **23** 495602

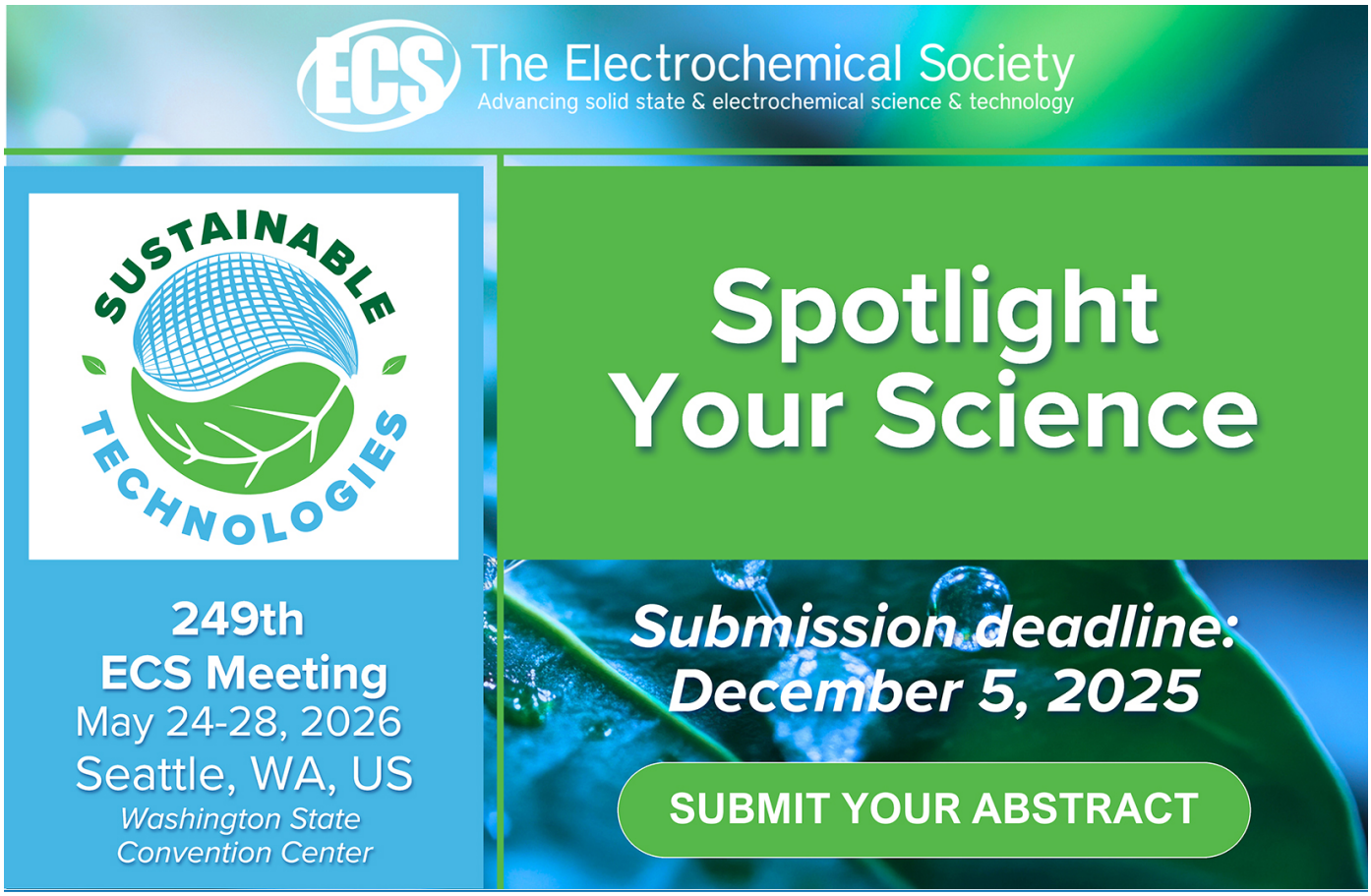

Nanotechnology **23** (2012) 495602 (10pp) doi:10.1088/0957-4484/23/49/495602

ZnO dense nanowire array on a film structure in a single crystal domain texture for optical and photoelectrochemical applications

Miao Zhong[1], Yukio Sato[2], Mario Kurniawan[1], Aleksandra Apostoluk[3], Bruno Masenelli[3], Etsuo Maeda[1], Yuichi Ikuhara[2] and Jean-Jacques Delaunay[1]

[1] School of Engineering, The University of Tokyo, 7-3-1 Hongo, Bunkyo-ku, Tokyo 113-8656, Japan
[2] Institute of Engineering Innovation, School of Engineering, The University of Tokyo, 2-11-16 Yayoi, Bunkyo-Ku, Tokyo 113-8656, Japan
[3] Institut des Nanotechnologies de Lyon (INL, CNRS UMR-5270), INSA Lyon, Université de Lyon, 7 Avenue Jean Capelle, Villeurbanne F-69621, France

E-mail: zhong.miao@scale.t.u-tokyo.ac.jp and jean@mech.t.u-tokyo.ac.jp

Received 24 August 2012, in final form 25 August 2012
Published 13 November 2012
Online at stacks.iop.org/Nano/23/495602

Abstract
A single crystal domain texture quality (a unique in-plane and out-of-plane crystalline orientation over a large area) ZnO nanostructure of a dense nanowire array on a thick film has been homogeneously synthesized on *a*-plane sapphire substrates over large areas through a one-step chemical vapor deposition (CVD) process. The growth mechanism is clarified: a single crystal [$0\bar{2}1$] oriented $ZnAl_2O_4$ buffer layer was formed at the ZnO film and the *a*-plane sapphire substrate interface via a diffusion reaction process during the CVD process, providing improved epitaxial conditions that enable the synthesis of the high crystalline quality ZnO nanowire array on a film structure. The high optoelectronic quality of the ZnO nanowire array on a film sample is evidenced by the free exitonic emissions in the low-temperature photoluminescence spectroscopy. A carrier density of $\sim 10^{17}$ cm^{-3} with an n-type conductivity of the ZnO nanowire array on a film sample is obtained by electrochemical impedance analysis. Finally, the ZnO nanowire array on a film sample is demonstrated to be an ideal template for a further synthesis of a single crystal quality ZnO–$ZnGa_2O_4$ core–shell nanowire array on a film structure. The fabricated ZnO–$ZnGa_2O_4$ sample revealed an enhanced anticorrosive ability and photoelectrochemical performance when used as a photoanode in a photoelectrochemical water splitting application.

(Some figures may appear in colour only in the online journal)

1. Introduction

Due to their unique optical, electrical and semiconducting properties, one-dimensional ZnO nanowire (NW) arrays have been extensively studied in the past decade for their potential use in electronic, photonic, electromechanical and electrochemical applications [1–6]. As ZnO is an abundant and cheap material, recent scientific studies focused on an efficient fabrication and assembly of high-quality ZnO NW arrays by simple and easy controllable methods which can be commercially competitive. Compared to some sophisticated technologies such as molecular beam epitaxy (MBE), atomic layer deposition (ALD) and electron beam lithography, chemical vapor deposition (CVD) and wet chemical growth

are substantially cost-effective methods [7–9], and, therefore, desirable for mass production of the ZnO NW arrays. However, multiple challenges still remain to be addressed, as far as these simple fabrication methods are concerned. One of the most difficult issues is the realization of a high texture quality of a ZnO NW array (i.e., a single crystal quality and a single crystal domain orientation over a large area) by a CVD or wet chemical process. A good texture quality is essential for the development of high-performance photonic, electronic and optoelectronic devices [10–12]. For example, a large decrease in the electron mobility from 120 to 30 $cm^2\ V^{-1}\ s^{-1}$ is obtained between a ZnO thin film with a unique crystalline domain and a ZnO thin film having two domains with distinct in-plane orientations [10]. This is explained as the result of the rotational defects in ZnO [10]. The decreased electron mobility may affect the charge collection efficiency, thus a high texture quality of the ZnO NW arrays is crucial to obtain enhanced performances in electronic, optoelectronic and piezoelectric devices.

Generally, epitaxial growth is a pre-requisite to achieve a high texture quality of the fabricated materials [10, 13–15]. GaN matches the in-plane geometry and lattice constants of ZnO, and therefore has been used as an epitaxial substrate for the growth of the ZnO NW arrays, regardless of the high cost of GaN single crystals. However, the unintentional doping of the ZnO NW array with Ga and/or N easily occurs during the growth processes [16], and this unintentional doping renders the electronic properties of the fabricated ZnO NWs difficult to control. On the other hand, the sapphire is a chemically stable and relatively cheap substrate material for the growth of ZnO NW arrays. However, two major issues need to be addressed for the ZnO NW array on the sapphire substrate to be applied in optoelectronic devices: (1) since sapphire is an electrical insulator, the ZnO NWs grown directly on the sapphire substrate are not electrically connected. Efficient electrical assembly of the fabricated ZnO NWs is required. (2) The epitaxial mechanism of the high-quality ZnO on the sapphire substrate is not fully clarified due to the large in-plane lattice mismatches existing between the ZnO and the sapphire substrate[4]. The understanding of the epitaxial mechanism of the ZnO on the sapphire is preferred to achieve a reliable growth of the high-quality ZnO crystals.

In this work, a nanowire array on a film structure consisting of dense and vertically aligned ZnO NWs on a thick ZnO film was synthesized on an *a*-plane sapphire substrate through a one-step CVD process. This simple CVD process enables the growth of a dense ZnO NW array on a thick ZnO film in the wurtzite-phase in a single-domain texture and highly oriented along the ZnO *c*-axis direction over a large area, as evidenced from the obtained transmission electron microscopy (TEM) images, selected area electron diffraction (SAED) patterns, x-ray diffraction (XRD) pole figures and XRD rocking curves. The epitaxial mechanism of this single-domain texture and *c*-oriented ZnO NW array on a ZnO film structure is elucidated: a single crystalline $ZnAl_2O_4$ buffer layer was found to be formed between the epi-ZnO film and the *a*-plane sapphire substrate. The well-oriented single crystal $ZnAl_2O_4$ buffer layer (with aligned crystallographic orientations of Al_2O_3 $[11\bar{2}0] \parallel ZnAl_2O_4[0\bar{2}1] \parallel ZnO[0001]$) provides an improved in-plane symmetry and reduced lattice mismatches, and, therefore favors the epitaxial growth of a high-quality ZnO NWs on a ZnO film structure. The understanding of the role of the $ZnAl_2O_4$ buffer layer in supporting the epitaxial growth of ZnO on the *a*-plane sapphire may have a profound impact on the growth techniques of single-domain and highly *c*-oriented ZnO films and nanostructures.

The optical and electronic properties of the fabricated ZnO NW array on a ZnO film structure were further characterized by low-temperature photoluminescence (PL) spectroscopy and electrochemical impedance spectroscopy. Free exciton and bound exciton emissions along with phonon replica emissions were clearly observed in the low-temperature PL spectrum, indicating a good crystalline quality of the fabricated ZnO NW array on a ZnO film structure. An n-type semiconductor behavior and the carrier density of $\sim 10^{17}$ cm^{-3} were obtained from the electrochemical impedance analysis. Finally, the fabricated ZnO NW array on a ZnO film sample resulted in being an ideal template for a subsequent synthesis of a single crystal ZnO–$ZnGa_2O_4$ core–shell NW array. The core–shell NW array on a film sample exhibited an enhanced anticorrosive and photo-oxidative performance when used as a photoanode in a photoelectrochemical water splitting cell. The one-step CVD technique is suitable for the large-scale fabrication of a single-domain and highly *c*-oriented ZnO NW array on a ZnO film structure and will contribute to the development of ZnO-based high-performance electronic, optical and optoelectronic devices.

2. Experimental details

The ZnO nanostructure of a dense ZnO NW array on a thick ZnO film was fabricated on *a*-plane sapphire substrates over a large area using a simple CVD process. An Au-coated *a*-plane sapphire was used as substrate and placed at the center of the CVD furnace tube. ZnO powder and graphite powder (0.2 g in weight) with a 2:1 weight ratio were loaded into an alumina boat as precursors and placed at a position 1 cm upstream from the substrate in the furnace tube. The furnace operated at 1000 °C for 30 min under argon and oxygen atmosphere (5:1 in volume ratio) flowing through at a working pressure of 50 mbar. Then the furnace cooled down to room temperature naturally. A dense ZnO NW array on a thick ZnO film structure was fabricated on the Au-coated *a*-plane sapphire substrate.

[4] The ideal *c* surface of ZnO is six-fold symmetric while the ideal *a* surface of sapphire is twofold symmetric, and thus they are essentially incompatible for epitaxial growth. On the lattice mismatch point of view, the ZnO *a* axis and the sapphire *c* axis are related by a factor of four, giving a small lattice mismatch of about 0.076%. However, the lattice mismatch on the other in-plane axis between ZnO$[1\bar{1}00]$ and sapphire $[1\bar{1}00]$ is large, reaching about 32%. Thus, a residual stress may exist at the interface of the ZnO *c* surface and the sapphire *a* surface, leading to the presence of misfit dislocations in the epi-grown ZnO film, which makes the epitaxial mechanism of high-quality *c*-oriented ZnO grown on the *a*-plane sapphire not fully understood.

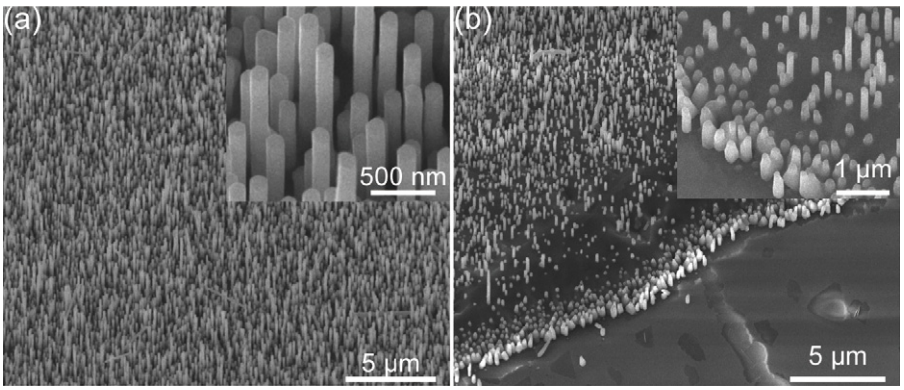

Figure 1. The morphology of the fabricated ZnO nanowire array on a ZnO film. (a) Tilted-angle SEM image of large-area dense and vertically aligned ZnO nanowires on the Au-coated *a*-plane sapphire substrate. Inset in (a) is a close-up of the vertically aligned ZnO nanowires. (b) Tilted-angle SEM image showing the structure of ZnO nanowires standing on the ZnO film at the edge area of the Au-coated *a*-plane sapphire surface. Inset in (b) is a close-up of the ZnO nanowire on a ZnO film structure at the Au-coated edge area.

Scanning electron microscopy (SEM) images of the fabricated ZnO NW array on a thick ZnO film sample were registered with a Hitachi S3000N microscope. Standard $\theta/2\theta$ scans, the x-ray diffraction rocking curves and x-ray pole figures measurements of the fabricated ZnO structures were made using the Smart lab XRD of Rigaku, Japan. TEM and STEM observations were carried out with JEOL JEM-2100F and ARM-200F microscopes and a JED-2300T EDS system. HAADF STEM images were acquired with the probe forming an aperture semiangle of ∼22 mrad and an inner detection angle greater than 70 mrad.

The electrochemical impedance measurements of the synthesized ZnO NW array on a ZnO film sample were performed with a Princeton Applied Research VersaSTAT 4 potentiostat. An electrolyte solution of 0.5 M $NaClO_4$ was prepared and buffered to a pH of 7.0 with the phosphate buffer solution. An Ag/AgCl electrode in the saturated KCl solution was used as a reference electrode, a Pt wire was used as a counter electrode and the ZnO NW array on a ZnO film sample was used as a working electrode. Before the electrochemical impedance measurement, N_2 gas was bubbled for 10 min to get rid of the O_2 in the electrolyte. The cyclic voltammetry and the Nyquist plots were at first registered in the dark in order to determine the appropriate range for the applied bias and the frequency applied to the electrode of the ZnO NW sample. Then, the Mott–Schottky analysis was performed in the dark with a bias varying from −0.4 to 0.4 V (versus the reference electrode) and at a frequency of 1 kHz.

3. Results and discussions

3.1. Morphology and texture quality of the ZnO nanowire array on a ZnO film

The morphology and structure of the synthesized ZnO NW array on a ZnO film are presented in the tilted-angle scanning electron microscopy (SEM) images. Figure 1(a) shows a highly uniform and densely assembled ZnO NW array grown over a large area on an Au-coated *a*-plane sapphire substrate. The inset in figure 1(a) is an enlarged SEM image of the vertically aligned ZnO NWs. The vertical alignment and smooth sidewalls of the ZnO NWs can be clearly observed. The average diameter of the ZnO NW is about 100 nm and the average length is about 1 μm. Figure 1(b) shows the morphology of the ZnO NW array on a ZnO film sample near the Au-coated edge area of the *a*-plane sapphire surface. The density of the NWs is low near the edge area so the underlying ZnO film can be noticed. Thus we can infer that the roots of the NWs are connected to the ZnO film underneath. Energy dispersive x-ray analyses (EDX) performed on the underlying ZnO film and on the NW array gave similar results: a Zn/O atomic ratio of about 1/1 was obtained, indicating that the NWs and the underlying film are made of ZnO.

Scanning transmission electron microscopy (STEM) was used to analyze the structure and the composition of the ZnO NW array on a ZnO film sample. Figure 2(a) shows a cross-sectional high-angle annular dark-field (HAADF) STEM image of the NW array on a ZnO film structure. The average length of the NWs is about 1 μm and the thickness of the film is about 2.5 μm. Energy dispersive spectroscopy (EDS) analyses were performed in STEM to examine the spatial distribution of the various chemical elements in the studied sample. The STEM–EDS mapping images presented in figure 2(b) show that the signal from the Al is confined in the substrate region and the signal from the Zn is confined in the nanowires and film region above the substrate, confirming that the structure of a ZnO NW array on a ZnO film is synthesized on the *a*-plane sapphire substrate. A magnified bright-field STEM image and STEM–EDS mapping images on the top region of the sample (see figure 2(c)) reconfirm the formation of vertically aligned ZnO NWs on the ZnO film.

Electron diffraction (ED) analyses in transmission electron microscopy (TEM) were further performed to characterize the crystalline quality and the crystallographic orientation of the ZnO NW array on a ZnO film sample. The ED pattern taken in the ZnO film region along the $[1\bar{1}00]$ zone axis (see figure 2(d)) shows that the ZnO thick film is single crystalline and well aligned along the [0001] direction of the wurtzite-phase. This feature can also be observed from the ED

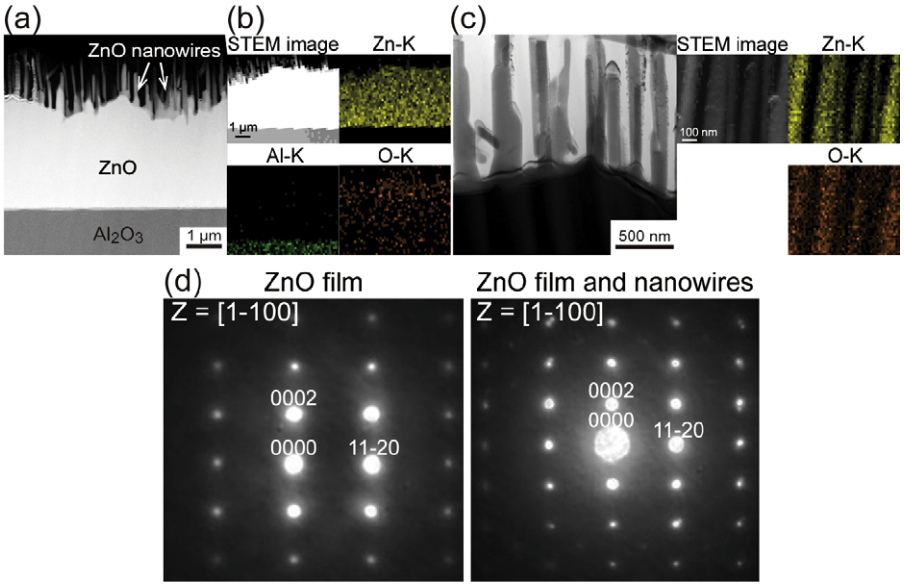

Figure 2. (a) HAADF STEM image of a cross-sectional view of the ZnO nanowire array on a ZnO film structure. (b) HAADF STEM image and EDS mapping images of the ZnO nanowire array on a ZnO film structure on the *a*-plane sapphire substrate. (c) Magnified bright-field STEM image of the ZnO nanowire array region (left); HAADF STEM image and Zn, O EDS mapping images of the ZnO nanowire array region (right). (d) Electron diffraction patterns taken in the region of the ZnO film (left) and in the region containing the ZnO film with ZnO nanowires (right).

pattern taken in the region containing the ZnO film and ZnO NWs (see figure 2(d)).

Since the ED technique is a local area analysis and provides information of the examined crystals within a small region defined by the TEM observation aperture (usually in the nanometer/micrometer range), it may happen that it does not represent the microstructure of the sample on a large scale. Thus a standard x-ray diffraction (XRD) $\theta/2\theta$ measurement was performed to examine the crystal structure and crystal plane orientations on a millimeter range. The XRD result presented in figure 3(a) shows two dominant diffraction peaks indexed as the wurtzite ZnO(0002) and (0004) planes. This result is evidence for the good crystallinity of the ZnO film and ZnO NWs and for their preferential growth orientation along the ZnO[0001] direction. The XRD θ rocking curve measurement of the ZnO(0002) peak is reported in figure 3(b). A small value of the full width at half maximum of 0.097° is obtained, indicating a perfect alignment of the ZnO crystalline domains in the [0001] direction.

We have demonstrated that the ZnO NW array on a ZnO film sample is of a single crystalline quality and well aligned along the ZnO[0001] crystallographic axis. However, a rotational degree of freedom around the ZnO[0001] axis has to be characterized [17]. Indeed, the texture of the sample could be either a unique crystal domain or a fiber domain. In the fiber domain-type structure, the orientations of the crystallographic axes normal to [0001] axis are not fixed and result in a fiber-like arrangement. The texture quality of the material is an important characteristic, determining its optical, optoelectronic, and mechanical properties [10, 17] (see footnote 4). To clarify the texture type of the fabricated NWs on a ZnO film sample, x-ray pole figure analysis was carried out. The x-ray pole figure measurement shown in figure 3(c) was performed on the ZnO NW array on a ZnO film sample with the ZnO($10\bar{1}2$) reflection. The scheme of the stereographic projection of the x-ray pole figure measurements is shown in figure 3(c). An alternative way to demonstrate the resulting pole figure is the azimuthal β scan curve covering the radial angle α from 0° to 90° presented in figure 3(c). A strong reflection intensity in the pole figure measurement is observed when the Euler angles (θ, α, β) of a sample placed in the goniometer satisfy the diffraction condition of its crystal structure [17]. A six-fold rotational symmetry of the ($10\bar{1}2$) reflections can clearly be seen in the resulting pole figure, implying that no (or very few) in-plane rotational domains or twins were present in the fabricated NW array on a ZnO film sample. Direct evidence for the single crystal domain of the ZnO NW array on a ZnO film sample is provided by the SEM top-view image shown in figure 3(d). It can be clearly noticed that the tips of the ZnO NWs form hexagons whose sides are perfectly aligned. Such an alignment of the hexagons can only be obtained if all ZnO NWs are homoepitaxially grown on a single crystalline domain ZnO film. It can also be noted that the hexagonal alignment is obtained over a large area. Thus, our synthesized sample of the ZnO NW array on a ZnO film is composed of a unique ZnO crystal domain, described by the texture orientation of {(0001)[$10\bar{1}0$]}, as depicted in figure 3(d).

3.2. Epitaxial growth mechanism of the ZnO nanowire array on a ZnO film

The heteroepitaxy of the ZnO film on the *a*-plane sapphire substrate is investigated in order to understand the growth mechanism of the ZnO epi-layer and to achieve a better control of the fabrication of high-quality and efficient ZnO

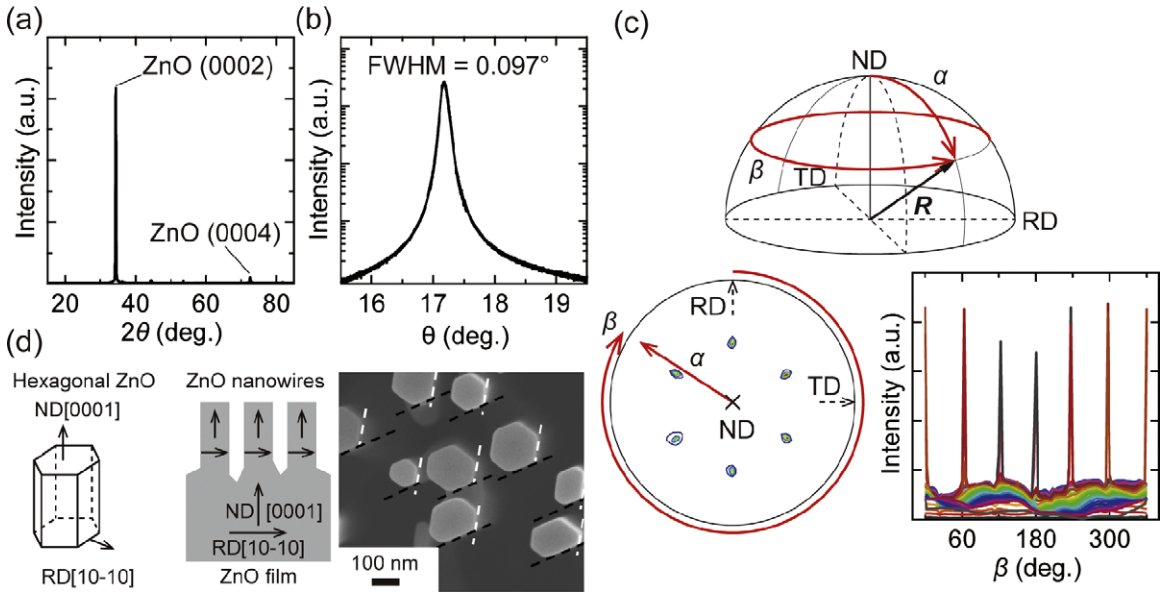

Figure 3. XRD analyses of the ZnO nanowire array on a ZnO film sample. (a) Standard XRD $\theta/2\theta$ measurement. (b) Rocking curve (intensity versus θ) around the ZnO(0002) diffraction peak. (c) Schematic drawing of the x-ray pole figure measurement (left); stereographic projections of the x-ray pole figure results for the ZnO($10\bar{1}2$) reflection (middle), color areas indicate higher diffraction intensity; azimuthal β curves of the x-ray pole figure result (right). ND: north-pole direction or normal direction; RD: rotational direction; TD: transverse direction. (d) Schematic of the ZnO crystal (left) and the ZnO nanowire array on a ZnO film having a unique crystal domain orientation (middle); top-view SEM image of the ZnO nanowires; a perfect alignment of the nanowires' hexagonal tips can be clearly seen (right).

nanostructures. As the problems of the unmatched geometry and a large one-axis lattice mismatch exist between the ZnO *c*-plane and the sapphire *a*-plane (see footnote 4), the epitaxial growth of a high-quality ZnO films or NWs on the sapphire substrates is not fully clarified. Therefore, the investigation of the interface between the ZnO epi-layer and the *a*-plane sapphire substrate is of great importance in order to understand the heteroepitaxial growth of a high-quality ZnO films or NWs on the *a*-plane sapphire.

In the HAADF STEM image of figure 2(a), an intermediate layer showing a different brightness contrast can be noticed between the ZnO film and the *a*-plane sapphire substrate. Note that in HAADF STEM imaging, the brightness in the image depends on the atomic number Z of the elements making up the sample [18]. A magnified HAADF STEM observation was further performed at the ZnO and the *a*-plane sapphire interface region, as shown in figure 4(a). The brightness of the intermediate layer is found to be in between that of the ZnO film and the sapphire, revealing that the 0.08 μm-thick intermediate layer is likely a diffusion layer having a different chemical composition. The Al, Zn, O K-shell EDS mapping images presented in figure 4(b) confirm that the intermediate layer contains Zn, Al, and O elements. Further, the ED pattern of the interface region shown in figure 4(d) taken along the zone axis of [112] gives two sets of single crystalline electron diffraction dots, identified as the spinel $ZnAl_2O_4$ and the sapphire. Hence, the intermediate layer is composed of a single crystalline spinel $ZnAl_2O_4$ with a [$0\bar{2}1$] crystallographic orientation, parallel to the [0001] direction of the ZnO film and parallel to the [$11\bar{2}0$] (see footnote 4) direction of the *a*-plane sapphire substrate, as illustrated in figure 4(c). Note that the ($0\bar{2}1$) plane of the spinel $ZnAl_2O_4$ has a trigonal crystalline symmetry that matches the hexagonal geometry of the wurtzite-phase ZnO *c*-plane and exhibits small lattice mismatches of 1.5% and 0.47% with the two crystallographic axes of the ZnO *c*-plane. In section 3.3, we discuss the possible growth mechanism of the high-quality and [0001] oriented ZnO film on the *a*-plane sapphire. An uniaxial heteroepitaxy first occurred to form a single orientational {(0001)[$10\bar{1}0$]} ZnO domain, due to the perfectly matched lattice constants between the ZnO *a*-axis and the sapphire substrate *c*-axis. The anisotropic nature of the crystal lattice in the *a*-plane of the sapphire helps to reduce the formation of the rotational domains within ZnO(0001) plane in the beginning of the growth process, as has been reported in the literature for the selected growth routes [10]. However, the large lattice mismatch induced in-plane stress in the axial direction between the ZnO[$1\bar{1}00$] and the sapphire [$1\bar{1}00$] becomes difficult to balance during the growth process. During our CVD growth of the ZnO NWs on a ZnO film sample, diffusion of Zn atoms into the sapphire substrate occurs, resulting in a formation of a single crystalline and [$0\bar{2}1$] oriented $ZnAl_2O_4$ intermediate layer. Thus, an optimized geometry of ZnO(0001) $\|$ $ZnAl_2O_4(0\bar{2}1)\|$ $Al_2O_3(11\bar{2}0)$ with an improved lattice matching, helps to reduce the residual stress at the ZnO–sapphire interface and supports the growth of a high-quality and [0001] oriented ZnO film. The formation of the $ZnAl_2O_4$ buffer layer is made possible by a diffusion reaction which requires a temperature of about 600 °C [19–21], a condition readily fulfilled under the growth conditions we apply (the temperature of the furnace is of about 1000 °C).

Note that the ZnO NW array on a ZnO film structure is only grown on the Au-coated surface area of the *a*-plane

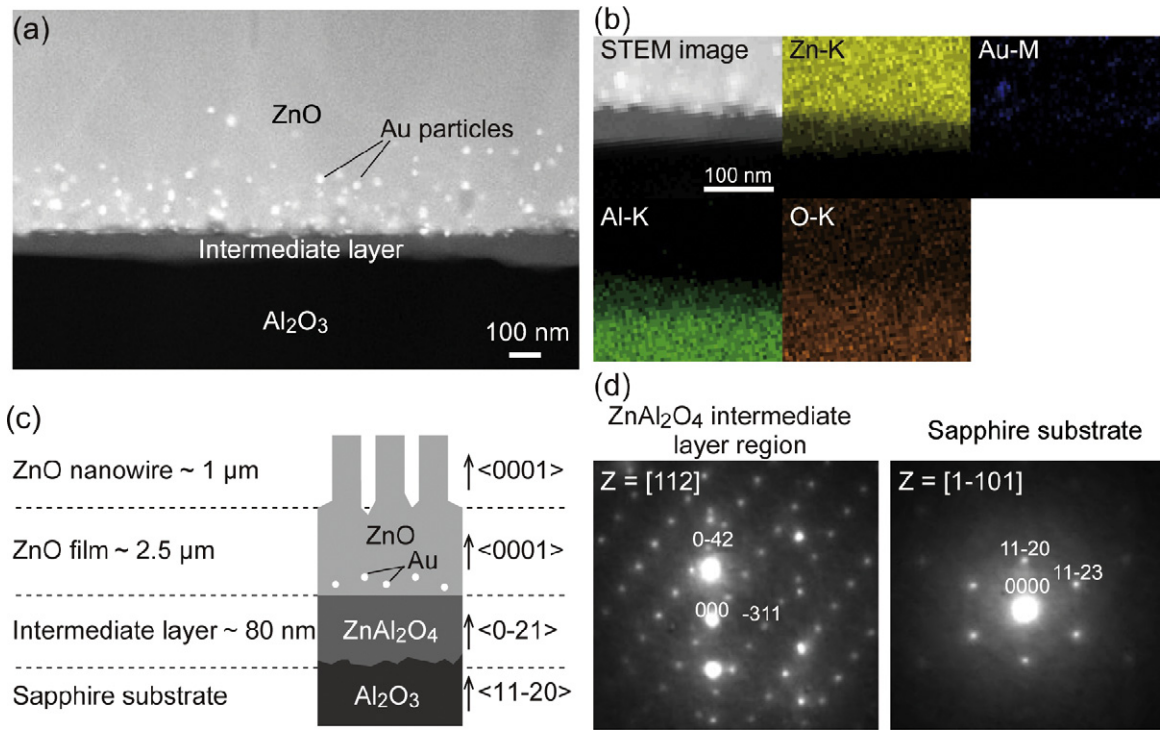

Figure 4. (a) HAADF STEM image of a magnified view at the interface of the ZnO film and the *a*-plane sapphire substrate. (b) HAADF STEM image and EDS mapping images taken in the interface region of the ZnO film and the sapphire substrate. (c) Schematic illustration of the ZnO nanowire array on a ZnO film structure showing aligned crystallographic orientations within each layer. (d) Electron diffraction patterns taken in the interface region of the ZnO film and the *a*-plane sapphire substrate and taken in the region of the *a*-plane sapphire substrate.

sapphire substrate, which indicates that the nucleation of ZnO on the surface of *a*-plane sapphire is difficult without the assistance of Au under our growth conditions. As reported [3–6], Au is an efficient catalyst which captures and localizes Zn and O vapor atoms, and thus contributes to the formation of ZnO nuclei in a conventional vapor–liquid–solid (VLS) process. This is due to a strong binding affinity between the Au atoms and ZnO [22]. Therefore, a schematic of the proposed growth process of our ZnO nanowire array on a film structure is shown in figure 5. In figure 5(a), the *a*-plane sapphire substrate was first deposited with Au particles by a quick coater. The sizes of the Au particles deposited on the *a*-plane sapphire substrate was measured using a dynamic force microscope (DFM) of SII (SPI 3800N/SPA-400). The estimated diameters of the as-deposited Au particles was about 10 nm (see the DFM image in figure 5(e)). With the increase of temperature in the CVD growth process, the Au particles on the *a*-plane sapphire substrate tended to migrate together to form large particles, as shown in figure 5(b). To prove the formation of large Au particles at elevated temperatures, an annealing experiment was performed. An *a*-plane sapphire deposited with the same amount of Au was annealed at 1000 °C for 15 s with Ar gas flowed through and without Zn and O sources at a pressure of 50 mbar. After the annealing process, the Au-deposited *a*-plane sapphire substrate cooled down to room temperature naturally. The SEM image of the annealed sample is shown in figure 5(e). Large Au particles were formed after the annealing process with estimated diameters of about 75 nm and 25 nm. In our ZnO growth process with the Zn and O sources, the enlarged Au particles captured the Zn and O vapor to form Au–Zn alloy particles at elevated temperatures and serves as a catalyst to facilitate the ZnO nucleation as shown in figure 5(c). Due to the presence of a sufficient supply of Zn and O vapor sources, a fast growth of the ZnO nanowires and the ZnO film occurred. It is suggested that the large Au–Zn alloy particles could meet the minimum diameter requirement for the growth of nanowire in a VLS growth process [23], and supported the growth of the ZnO nanowires. During the growth of the ZnO nanowires, Au may migrate away from its original location because Au has a high diffusion rate at high growth temperature [4, 24, 25]. In our process, it is very probable that Au atoms diffused from the Au-rich area to the area with low Au density on the surface of the ZnO nanowires and ZnO film. In consequence, the ZnO nanowires stopped the growth without the sufficient support of Au catalysts, and, therefore a Au-catalyzed VLS growth process explained the growth of the ZnO nanowires. In addition, a large amount of Au particles with smaller diameters were also formed on the surface of the *a*-plane sapphire substrate at the initial stage of the high-temperature CVD process. The smaller Au particles captured the Zn and O sources to form ZnO nuclei and supported the growth of the ZnO film. This hypothesis is confirmed with the STEM and EDS analyses of the fabricated ZnO sample. Many Au particles with diameters of about 10–30 nm were buried at the very bottom of the ZnO film,

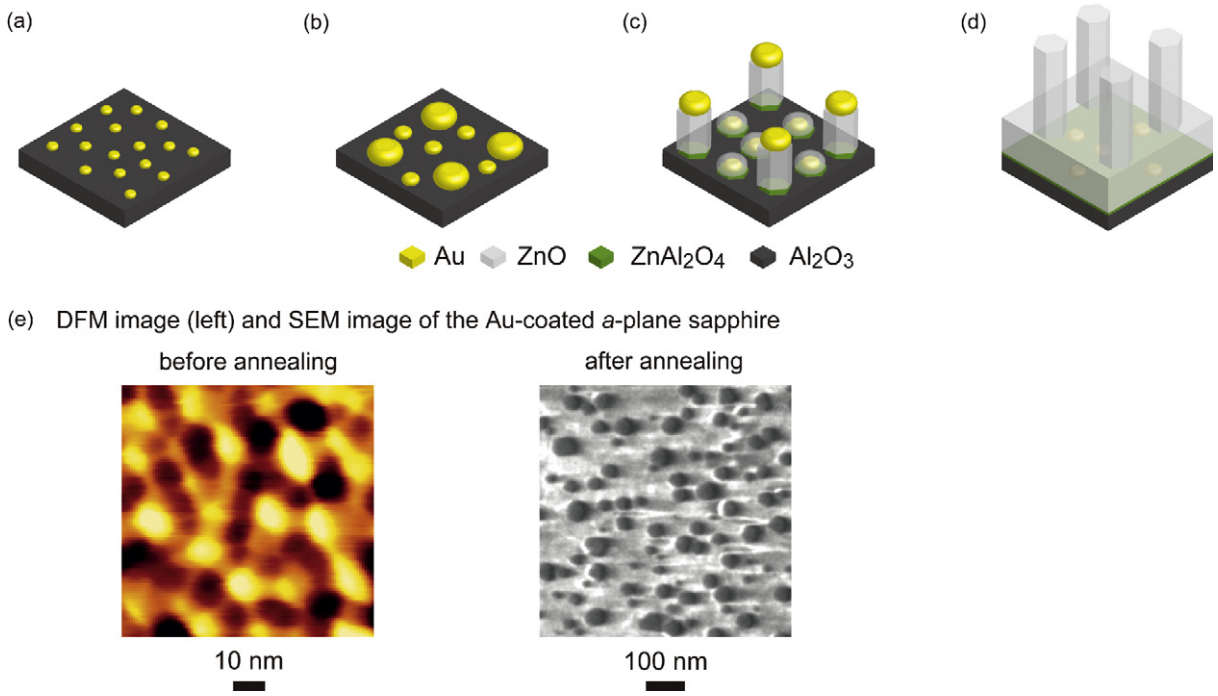

Figure 5. (a)–(d) Schematic drawing of the CVD growth process of the ZnO nanowire array on a ZnO film structure on the *a*-plane sapphire substrate. (a) Au particles was deposited on the *a*-plane sapphire substrate. (b) Large Au particles were formed at elevated temperatures during the CVD process. (c) Au particles captured Zn and O vapor atoms to form the ZnO nuclei. The large droplets supported the growth of the ZnO nanowires and the small droplets supported the growth of the ZnO film. The $ZnAl_2O_4$ buffer layer was also formed at the interfaces between the ZnO and the sapphire substrate. (d) The ZnO nanowire array on a ZnO film structure was formed after the CVD growth. (e) DFM and SEM images of the Au particles on the *a*-plane sapphire substrate before and after an annealing process. The annealing process of the Au-coated *a*-plane sapphire substrate was operated at 1000 °C for 15 s with only argon gas flowed through at a pressure of 50 mbar.

as shown in the HAADF STEM image of figure 4(a). Au nanoparticles are detected as strong brightness contrast in figure 4(a) due to the large difference in Z between Au and other elements [18]. The presence of Au nanoparticles in the vicinity of the interface on the ZnO film was further confirmed by Au M-shell EDS analysis in figure 4(b). After the CVD growth process, the ZnO nanowire array on a film structure was formed on the *a*-plane sapphire substrate, as shown in figure 5(d).

The low-temperature PL spectrum excited with a He–Cd UV laser operating at 325 nm was measured at 13 K and permitted to characterize the optical quality of the studied structures. The PL spectrum presented in a semi-log scale in figure 6 shows one dominant peak emission in the 3.35–3.36 eV region. This sharp and intense peak is attributed to the neutral-donor-bound exciton line (D^0X) of ZnO. On the high-energy side of this peak, the ZnO A-free exciton at $FX_A^{n=1} = 3.37$ eV can be observed. The first excited state emission of the A-free exciton at $FX_A^{n=2} = 3.42$ eV can be observed unambiguously. The observation of the A-free exciton and its first excited state emission is clear evidence that the ZnO NW array on a ZnO film sample is of a high crystalline quality and essentially free of strain. Furthermore, fine structures related to longitudinal optical (LO) phonon replica lines of the dominant neutral-donor-bound exciton D^0X emission and the A-free exciton of $FX_A^{n=1}$ are clearly seen in the spectrum presented in figure 6. The first-order (1LO), second-order (2LO), and third-order (3LO) replicas of the D^0X emission and the first-order (1LO) and second-order (2LO) replicas of the A-free exciton of $FX_A^{n=1}$ are shifted by ∼70 meV towards lower energies from the main D^0X and $FX_A^{n=1}$ emission peaks. The two-electron satellite transition of $(D^0X)_{2e}$, characteristic of the neutral-donor-bound exciton transition is identified at ∼30 meV below the energy of the D^0X emission peak. All the positions of the emission peaks are in good agreement with literature reports for high-quality ZnO films and/or 1D nanostructures [4, 26, 27]. The PL properties indicate that high-quality ZnO NWs on a ZnO film were synthesized thanks to the formation of a single crystal $ZnAl_2O_4$ buffer layer between the sapphire substrate and the ZnO film, which helps to diminish the strain present in the ZnO layer due to the lattice constant mismatch between ZnO and the *a*-plane sapphire.

Electrochemical impedance spectroscopy was used to investigate the charge carrier density in the ZnO NW array on a ZnO film sample. Typically, carrier density values ranging from 10^{16} to 10^{18} cm^{-3} are reported in the literature for the undoped ZnO films or nanostructures fabricated by the gas-phase deposition methods [28, 29]. For the aqueous chemical deposition methods, an increased carrier density of 10^{19}–10^{20} cm^{-3} is usually observed, likely because of the unintentional doping of the ZnO NWs with hydrogen. This has been evidenced by the effect of the post-annealing treatment of the samples, in which the carrier density reduction to the range of 10^{16}–10^{18} cm^{-3} was

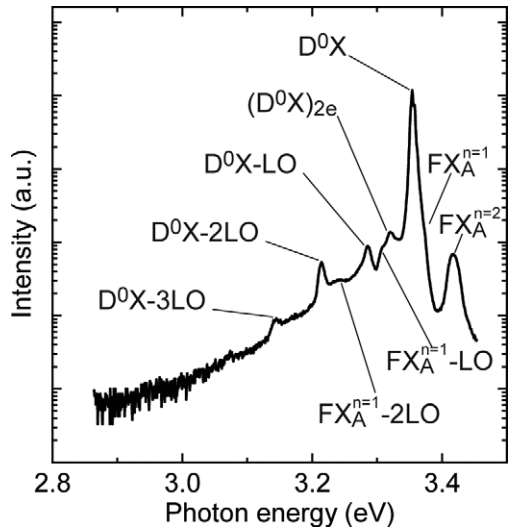

Figure 6. Low-temperature PL spectra performed at 13 K of the ZnO nanowire array on a ZnO film sample plotted in a semi-logarithmic scale.

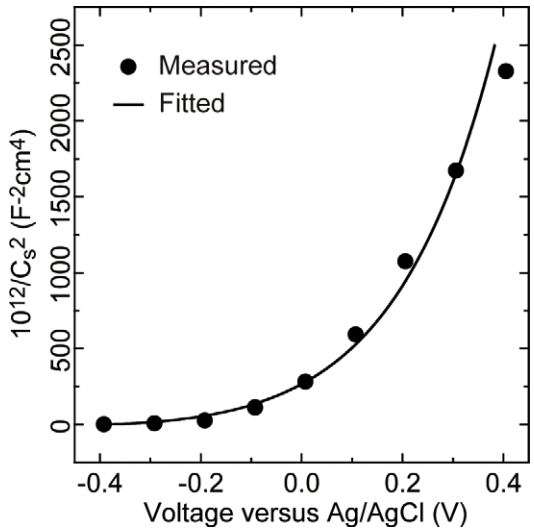

Figure 7. The Mott–Schottky plot of the ZnO nanowire on a ZnO film sample taken at a frequency of 1 kHz under dark conditions for a bias voltage ranging from −0.4 to 0.4 V (versus Ag/AgCl electrode).

observed due to the exodiffusion of the hydrogen during the post-annealing [30]. In our study, a calculated carrier density of about 10^{17} cm^{-3} with a n-type conductivity is obtained for the ZnO NW array on a ZnO film sample via fitting of the Mott–Schottky data using the Mora-Sero model [30], as shown in figure 7.

3.3. Photoelectrochemical applications of the ZnO nanowire array on a ZnO film

To sum up, we demonstrate a cost-effective method for the fabrication of a dense ZnO NW array on a ZnO film structure having a single crystal domain quality on the *a*-plane sapphire substrate. This technique can be applied to large-scale fabrication of high-quality ZnO NW arrays and may substantially reduce the cost and make easier the integration of ZnO NW arrays in electronic, optoelectronic, electrochemical and electromechanical applications. In addition, the ZnO NW array on a ZnO film structure is an ideal host to realize a broad range of functional materials by post-process doping or hetero-growth in the radial direction of the NWs, forming a ZnO-based core–shell nanowire array on a film structure. The usefulness of this nanowire array on a film structure is dictated by the realization of an efficient electrical charge collection because the nanowire and the film are made of same material with high crystal quality.

In the following, we used the ZnO NW array on a ZnO film sample as a template for the fabrication of a dense ZnO–$ZnGa_2O_4$ core–shell NW array on a ZnO film in the second CVD growth process. The synthesized ZnO–$ZnGa_2O_4$ core–shell NW array on a ZnO film sample permits an easy charge carrier collection through its thick bottom conductive film and has a stable and efficient photo-oxidation ability when used as a photoanode in a photoelectrochemical (PEC) water splitting cell [6]. The ZnO–$ZnGa_2O_4$ core–shell NWs are perfectly arranged, tightly packed and bonded altogether at their bases through the same material over large areas, as shown in the SEM image presented in figure 8(a). The ZnO–$ZnGa_2O_4$ core–shell NWs are single crystalline, with their crystallographic orientations aligned along $ZnGa_2O_4$ [111] ‖ ZnO[0002] [31].

The PEC performance of the ZnO–$ZnGa_2O_4$ core–shell nanostructured photoanode was investigated in a non-sacrificial agent of a 0.1 M Na_2SO_4 electrolyte solution at pH = 6 and under illumination with a 300 W xenon lamp. An Ag/AgCl electrode in a saturated KCl solution was used as a reference electrode and a Pt wire served as a counter electrode. The *I*–*V* measurement of the ZnO–$ZnGa_2O_4$ photoanode at an applied potential of 0.7 V (versus Ag/AgCl electrode) was performed for 15 min. As shown in figure 8(b), a low current density of $<10^{-4}$ mA cm^{-2} was obtained in the dark and a high and stable current of 1.2 mA cm^{-2} was measured under illumination with the xenon lamp for 15 min. The stable photocurrent observed under continuous light illumination revealed that the $ZnGa_2O_4$ shells worked as an anticorrosive outer-layer of the ZnO NWs, enhancing the stability of the photoanode in comparison to the ZnO or n-doped ZnO NWs, whose PEC performances deteriorate under continuous light illumination [2].

4. Conclusions

In summary, an easily controlled one-step CVD approach has been developed for a large-scale fabrication of the dense ZnO NW array on a ZnO film structure on the *a*-plane sapphire substrate, assisted with Au acting as a catalyst. The XRD pole figure and XRD rocking curve analyses revealed that the ZnO NW array on a ZnO film structure consists of a single crystal domain with the ZnO *c*-axis aligned perpendicularly to the *a*-plane sapphire substrate. STEM–EDS mapping and TEM ED studies also confirm the formation of a single crystal ZnO domain and the existence of a spinel $ZnAl_2O_4$

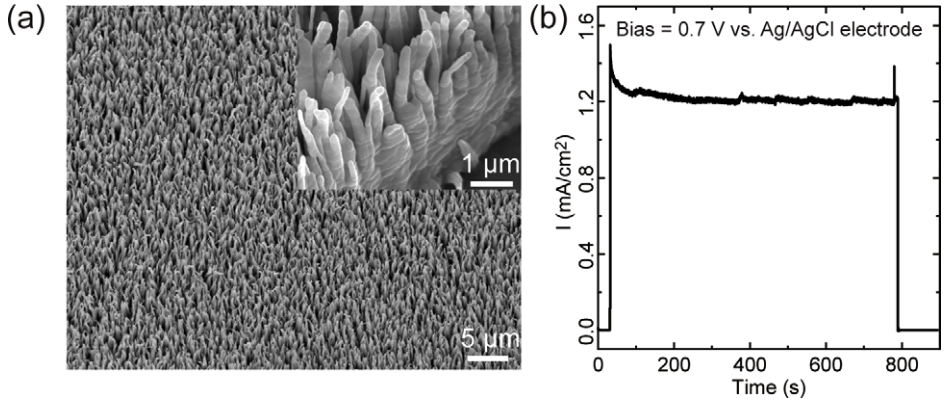

Figure 8. (a) Tilted-angle SEM image of a dense ZnO–$ZnGa_2O_4$ core–shell nanowire array. Inset in (a) is a close-up of the vertically aligned ZnO–$ZnGa_2O_4$ nanowires showing their roots bonded to the ZnO underlying film. (b) An *I–V* curve of the ZnO–$ZnGa_2O_4$ core–shell nanowire array on a ZnO film sample used as a photoanode at an applied bias of 0.7 V (versus Ag/AgCl) under illumination with a xenon lamp for about 15 min.

intermediate layer with the $[0\bar{2}1]$ orientation between the epi-ZnO film and the *a*-plane sapphire substrate. The matched in-plane symmetry and an improved lattice matching between the spinel $ZnAl_2O_4(0\bar{2}1)$ layer and the wurtzite ZnO(0001) film diminishes the possible strain present in the ZnO film and explains the high-quality epitaxial growth of the ZnO nanostructures. Both free and bound exciton emissions along with fine-featured phonon replica emissions are clearly observed in the low-temperature PL spectrum, indicating a good crystalline quality of the fabricated ZnO structure. The studied ZnO structures exhibit an n-type conductivity and a carrier density of $\sim 10^{17}$ cm^{-3}, as determined by the electrochemical impedance analysis. Finally, we report the application of the ZnO NWs on a ZnO film structure as a template for the fabrication of a single crystal ZnO–$ZnGa_2O_4$ core–shell NW array. The ZnO–$ZnGa_2O_4$ core–shell NW array on a film reveals an improved anticorrosive ability and an enhanced photoelectrochemical performance when used as a photoanode in a PEC water splitting cell. We expect the proposed ZnO NWs fabrication technique to provide an easy and reliable approach for the large-scale fabrication of high-quality single crystalline domain ZnO nanostructures. We are convinced that such a straightforward fabrication technique will contribute efficiently to the integration of the ZnO nanostructures in devices with an enhanced light collection and light emission ability, such as photovoltaic cells, photoelectrochemical cells and light emitting diodes.

Acknowledgments

This work was supported through the Grant-in-Aid for Scientific Research (B) 22360056 from the Japan Society for the Promotion of Science (JSPS) and Ministry of Education, Culture, Sports, Science and Technology (MEXT), the Grant-in-Aid from the Asahi Glass Foundation, the Grant-in-Aid for JSPS Fellows and the Global COE program, 'Global Center of Excellence for Mechanical Systems Innovation' by MEXT. Part of this work was also conducted in the Research Hub for Advanced Nano Characterization, The University of Tokyo, supported by MEXT, Japan.

References

[1] Wang X, Song J, Summers C J, Ryou J H, Li P, Dupuis R D and Wang Z L 2009 *J. Phys. Chem.* B **110** 7720
[2] Yang X, Wolcott A, Wang G, Sobo A, Fitzmorris R C, Qian F, Zhang J Z and Li Y 2009 *Nano Lett.* **9** 2331
[3] Zhang X X, Zhao D, Gao M, Dong H B, Zhou W Y and Xie S S 2011 *Nanotechnology* **22** 135603
[4] Fan H J *et al* 2006 *Small* **2** 561
[5] Yang P, Yan H, Mao S, Russo R, Johnson J, Saykally R, Morris N, Pham J, He R and Choi H 2002 *Adv. Funct. Mater.* **12** 323
[6] Zhong M, Li Y, Yamada I and Delaunay J-J 2012 *Nanoscale* **4** 1509
[7] Vayssieres L 2003 *Adv. Mater.* **15** 464
[8] Tian Z R, Voigt J A, Liu J, Mckenzie B, Mcdermott M J, Rodriguez M A, Konishi H and Xu H 2003 *Nature Mater.* **2** 821
[9] Baxter J B and Aydil E S 2005 *J. Cryst. Growth* **274** 407
[10] Fons P, Iwata K, Yamada A, Matsubara K, Niki S, Nakahara K, Tanabe T and Takasu H 2000 *Appl. Phys. Lett.* **77** 1801
[11] Volk J, Nagata T, Erdélyi R, Bársony I, Tóth A L, Lukács I E, Czigány Zs, Tomimoto H, Shingaya Y and Chikyow T 2009 *Nanoscale Res. Lett.* **4** 699
[12] Teo S H G, Liu A Q, Singh J, Yu M B and Lo G Q 2007 *Appl. Phys.* A **89** 417
[13] Fan H J, Lee W, Scholz R, Dadgar A, Krost A, Nielsch K and Zacharias M 2005 *Nanotechnology* **16** 913
[14] Park W I, Kim D H, Jung S W and Yi G 2002 *Appl. Phys. Lett.* **80** 4232
[15] Chen Y, Bagnall D M, Koh H, Park K, Hiraga K, Zhu Z and Yao T 1998 *J. Appl. Phys.* **84** 3912
[16] Levin I, Davydov A, Nikoobakht B, Sanford N and Mogilevsk P 2005 *Appl. Phys. Lett.* **87** 103110
[17] Engler O and Randle V 2010 *Introduction to Texture Analysis: Macrotexture, Microtexture, and Orientation Mapping* 2nd edn (Boca Raton, FL: CRC Press), (London: Taylor and Francis)
[18] Pennycook S J and Jesson D E 1990 *Phys. Rev. Lett.* **64** 938
[19] Yang Y, Kim D S, Knez M, Scholz R, Berger A, Pippel E, Hesse D, Gösele U and Zacharias M 2008 *J. Phys. Chem.* C **112** 4068
[20] Grabowska J, Kumar R R T, McGlynn E, Nanda K K, Newcomb S B, McNally P J, O'Reilly L, Mosnier J P and Henry M O 2008 *Thin Solid Films* **516** 1725
[21] Wang Y, Liao Q, Lei H, Zhang X, Ai X, Zhang J and Wu K 2006 *Adv. Mater.* **18** 943

[22] Polacer K and Wassermann E F 1976 *Thin Solid Films* **37** 65
[23] Wagner R S and Ellis W C 1965 *Trans. Metall. Soc. AIME* **4** 89
[24] Hannon J B, Kodambaka S, Ross F M and Tromp R M 2006 *Nature* **440** 69
[25] Kim D S, Scholz R, Gösele U and Zacharias M 2008 *Small* **4** 1651
[26] Teke A, Özgür Ü, Doğan S, Gu X and Morkoc H 2004 *Phys. Rev.* B **70** 195207
[27] Meyer B K *et al* 2004 *Phys. Status Solidi* b **241** 231
[28] Wolcott A, Smith W A, Kuykendall T R, Zhao Y and Zhang J Z 2009 *Adv. Funct. Mater.* **19** 1849
[29] Allen M W, Alkaisi M M and Durbin S M 2006 *Appl. Phys. Lett.* **89** 103520
[30] Mora-Seró I, Fabregat-Santiago F, Denier B and Bisquert J 2006 *Appl. Phys. Lett.* **89** 203117
[31] Zhong M, Li Y, Tokizono T, Yamada I and Delaunay J-J 2012 *J. Nanopart. Res.* **14** 804